

# Effects of drop freezing on microphysics of an ascending cloud parcel under biomass burning conditions

K. Diehl<sup>a,\*</sup>, M. Simmel<sup>b</sup>, S. Wurzler<sup>c</sup>

<sup>a</sup>*Institute of Atmospheric Physics, Johannes Gutenberg University, Becherweg 21, 55099 Mainz, Germany*

<sup>b</sup>*Leibniz Institute for Tropospheric Research, Leipzig, Germany*

<sup>c</sup>*North Rhine Westphalia State Environment Agency, Essen, Germany*

Received 25 April 2006; received in revised form 1 August 2006; accepted 4 August 2006

---

## Abstract

There is some evidence that the initiation of warm rain is suppressed in clouds over regions with vegetation fires. Thus, the ice phase becomes important as another possibility to initiate precipitation. Numerical simulations were performed to investigate heterogeneous drop freezing for a biomass-burning situation. An air parcel model with a sectional two-dimensional description of the cloud microphysics was employed with parameterizations for immersion and contact freezing which consider the different ice nucleating efficiencies of various ice nuclei. Three scenarios were simulated resulting to mixed-phase or completely glaciated clouds. According to the high insoluble fraction of the biomass-burning particles drop freezing via immersion and contact modes was very efficient. The preferential freezing of large drops followed by riming (i.e. the deposition of liquid drops on ice particles) and the evaporation of the liquid drops (Bergeron–Findeisen process) caused a further decrease of the liquid drops' effective radius in higher altitudes. In turn ice particle sizes increased so that they could serve as germs for graupel or hailstone formation. The effects of ice initiation on the vertical cloud dynamics were fairly significant leading to a development of the cloud to much higher altitudes than in a warm cloud without ice formation.

© 2006 Elsevier Ltd. All rights reserved.

*Keywords:* Biomass burning; Heterogeneous drop freezing; Ice nuclei; Mixed-phase cloud

---

## 1. Introduction

Biomass burning is one of the main sources of atmospheric aerosol particles (Levine, 1991). The fire induced convection transfers soils from the ground as well as burned and unburned vegetation fragments into the atmosphere. Field measurements indicate that particles from biomass burning consist of biogenic, pyrogenic, and soil dust components with

a high insoluble fraction between 80% and 95% (Artaxo et al., 1998; Feingold et al., 2001, Guyon et al., 2003). The number size distributions of these particles show large amounts of small particles (Helsper et al., 1980; Reid et al., 1998). Such particle distributions ingested in clouds lead to the formation of a large number of small drops. Thus, biomass burning can cause the suppression of warm rain as the formation of precipitation from these small drops by collision and coalescence is hardly possible (Rosenfeld, 1999; Andreae et al., 2004). However, another way to form precipitation is the ice phase.

---

\*Corresponding author.

E-mail address: [kdiehl@uni-mainz.de](mailto:kdiehl@uni-mainz.de) (K. Diehl).

In a temperature range between 0 and  $-35^{\circ}\text{C}$  primary ice in clouds is mostly formed by heterogeneous freezing, i.e. by particles containing an insoluble residue or consisting completely of insoluble material. Owing to their composition these ice nuclei initiate freezing at significantly different temperatures, leading to the formation of mixed phase clouds. An important way to form ice particles heterogeneously in the atmosphere is the freezing of super-cooled drops in immersion and contact modes (Pruppacher and Klett, 1997). For heterogeneous initiation of the ice phase the preconditions are fairly good in biomass burning clouds: The very high insoluble fraction of biomass burning particles potentially enhances ice formation (Diehl et al., 2006), and it contains particles which are known as efficient ice nuclei, i.e. black carbon, minerals, and biological particles (Artaxo et al., 1998; Guyon et al., 2003). On the other hand, both immersion and contact freezing show a preferential freezing of large drops (Diehl and Wurzler, 2004; Diehl et al., 2006). Thus, important questions are if under biomass burning conditions freezing of super-cooled drops occurs, if it is sufficient to affect the vertical cloud dynamics, and if precipitation-sized ice particles could form. In the present simulations, drop formation in clouds under biomass burning conditions was compared to activation of various aerosol particle number size distributions in clouds under cleaner conditions. Ice formation in the biomass burning clouds was simulated considering the portioning of the particles and their ice nucleating efficiency. A sectional cloud model with a detailed two-dimensional description of warm and cold microphysics was employed (Simmel and Wurzler, 2006; Diehl et al., 2006).

## 2. Model description

For the present simulations an adiabatic air parcel model with entrainment (Flossmann et al., 1985; Pruppacher and Klett, 1997) was employed. An air parcel model describes a rising bubble of air whose radius increases with height. Dry air is mixed with moist air into the parcel through entrainment. The advantage of an air parcel model is that all changes in the microphysical evolution of the cloud can be attributed to microphysical processes. On the other hand, this can only be achieved for a tradeoff in cloud dynamics including some well-known weaknesses in the treatment of precipitation sized cloud particles which stay inside the parcel. How-

ever, for the present case of biomass burning cloud drops typically remain rather small. Therefore, the more important limiting factor is the rather simple cloud dynamics.

The employed model includes warm and cold cloud microphysics and the interactions between aerosol particles and hydrometeors (Simmel and Wurzler, 2006; Diehl et al., 2006). The aerosol particles are internally mixed with variable insoluble and soluble fractions. The sectional description of cloud microphysics includes a number of warm microphysical processes such as growth and shrinking of aerosol particles by water vapor diffusion, impaction scavenging, drop nucleation, growth, evaporation, collision and coalescence. A state-of-the-art iterative condensation scheme is implemented. The entrainment of aerosol particles, drops, ice particles, temperature, and humidity is embedded (Simmel et al., 2005). The cold microphysics includes the freezing of drops in immersion and contact modes as primary freezing processes (Diehl and Wurzler, 2004; Diehl et al., 2006). Both descriptions for immersion and contact freezing consider the ice nucleation efficiency of different particle types. Condensation freezing is included implicitly in immersion freezing as drops which are nucleated during the ascent of the air parcel by entrained aerosol particles could freeze immediately by immersion freezing. Deposition freezing, i.e. ice nucleation directly from the vapour phase, and homogeneous freezing of super-cooled drops are both neglected in the present model simulations because heterogeneous freezing via immersion, condensation, and contact modes are the dominant freezing processes for the present situation of biomass burning with a large amount of potential ice nuclei. Deposition freezing takes place at lower temperatures than the other heterogeneous freezing processes, homogeneous freezing at significantly lower temperatures than all heterogeneous freezing processes (Schaller and Fukuta, 1979; Koop et al., 1999).

In the immersion mode, the freezing rate for pure water drops of same sizes containing insoluble particles is given by

$$-\frac{dN_f}{dt} = N_u a B_{h,i} V_d \exp(-aT) \frac{dT}{dt}, \quad (1)$$

where  $N_f$  is the number of frozen drops,  $N_u$  the number of unfrozen drops,  $V_d$  the drop volume in  $\text{cm}^3$ ,  $T$  the temperature in  $^{\circ}\text{C}$ ,  $a$  and  $B_{h,i}$  constants with  $a = 1^{\circ}\text{C}^{-1}$ . The constant  $B_{h,i}$  in  $\text{cm}^{-3}$  stands

for the ice nucleating efficiency in the immersion mode of an insoluble particle per unit volume of liquid. The freezing rate is coupled with an approach for the freezing point depression. For details see Diehl and Wurzler (2004). In the contact mode, the number of drops freezing at a temperature  $T$  when colliding with an insoluble particle is given by

$$N_f = -N_0(a_{h,c}T + b_{h,c}), \quad (2)$$

where  $T$  is the temperature in °C,  $a_{h,c}$  and  $b_{h,c}$  are constants. The constant  $a_{h,c}$  is in °C<sup>-1</sup>,  $b_{h,c}$  dimensionless. The freezing equation is coupled with an approach for collisions between super-cooled drops and dry aerosol particles. For details see Diehl et al. (2006). Drops frozen via contact and immersion (and implicitly via condensation) modes grow further by the deposition of water vapor and by the collision with super-cooled liquid drops (Diehl et al., 2006). The two-dimensional size distribution used for the microphysics is divided into 90 categories for the particulate mass and into 66 categories for the water mass, both starting with 0.002 μm in diameter, with a mass doubling in every category for the water mass and a mass doubling in every other category for the particulate mass. This combination is recommended in Simmel and Wurzler (2006).

### 3. Initial conditions and scenarios

The present model simulations were initialized with conditions typical for biomass burning situations. Two initial aerosol particle size distributions were selected: the young biomass burning distribution of Helsper et al. (1980) and the haze distribution of Reid et al. (1998). The distribution of Helsper et al. (1980) is a bimodal distribution, the

one of Reid et al. (1998) is a type of aged biomass burning aerosol, i.e. the particle sizes are shifted towards larger sizes and the numbers are reduced. The parameters of the particle distributions are given in Table 1. Biomass burning conditions were simulated by using the distribution of Helsper et al. (1980) for the parcel and the distribution of Reid et al. (1998) for the environment, young biomass burning conditions were simulated by using the distribution of Helsper et al. (1980) for both, the parcel and the environment (see Table 2). The particle concentrations of the environment were assumed to be constant with height. This is reasonable for the biomass burning cases where the aerosol particles are small and, therefore, do not experience a significant decrease in number with height (Khain et al., 2000). The model simulations for the clean cases may overestimate the number of entrained aerosol particles and, thus, the number of newly activated droplets. The vertical profiles of temperature and humidity used in the present simulations (see Fig. 1) were calculated with the regional model REMO for an area in Indonesia with biomass burning (Langmann, 2004, pers. comm.). The initial size of the air parcel was 4 km in diameter, a typical updraft size induced by vegetation fires, the temperature difference between the air parcel and the environment was set to 2 K. The soluble fraction  $\varepsilon$  of the particles was set 20%, i.e.  $\varepsilon = 0.2$  (Guyon et al., 2003), the soluble fraction of the aerosol particles consisted of ammonium sulfate. The insoluble fraction was assumed to contain a fraction of active ice nuclei. The estimations of these fractions are based on the measurements of Artaxo et al. (1998) and Guyon et al. (2003) who determined the source apportionment of aerosol particles during the dry season in the Amazonas

Table 1  
Parameters of initial aerosol particle number size distributions

Particle type	Parameters
Young biomass burning (Helsper et al., 1980)	$N_1 = 9000 \text{ cm}^{-3}$ , $d_1 = 0.015 \text{ } \mu\text{m}$ , $\sigma_1 = 1.5$ $N_2 = 1000 \text{ cm}^{-3}$ , $d_2 = 0.06 \text{ } \mu\text{m}$ , $\sigma_2 = 1.8$
Haze (Reid et al., 1998)	$N = 6000 \text{ cm}^{-3}$ , $d = 0.1 \text{ } \mu\text{m}$ , $\sigma = 1.65$
Rural background (Jaenicke, 1988)	$N_1 = 6650 \text{ cm}^{-3}$ , $d_1 = 0.004 \text{ } \mu\text{m}$ , $\sigma_1 = 1.7$ $N_2 = 147 \text{ cm}^{-3}$ , $d_2 = 0.013 \text{ } \mu\text{m}$ , $\sigma_2 = 3.6$ $N_3 = 1990 \text{ cm}^{-3}$ , $d_3 = 0.022 \text{ } \mu\text{m}$ , $\sigma_3 = 1.84$
Marine with continental influence (Hoppel and Frick, 1990; Hoppel et al., 1990)	$N_1 = 100 \text{ cm}^{-3}$ , $d_1 = 0.0135 \text{ } \mu\text{m}$ , $\sigma_1 = 1.8$ $N_2 = 120 \text{ cm}^{-3}$ , $d_2 = 0.052 \text{ } \mu\text{m}$ , $\sigma_2 = 1.3$ $N_3 = 12 \text{ cm}^{-3}$ , $d_3 = 0.06 \text{ } \mu\text{m}$ , $\sigma_3 = 2.8$

$N_i$  is the particle number,  $d_i$  the diameter, and  $\sigma_i$  the standard deviation of the respective mode  $i$ .

Table 2  
Description of all case studies

	AP parcel	AP environment	$\varepsilon$	IN
<i>Warm cases</i>				
Young biomass burning	Young biomass burning	Young biomass burning	0.2	No
Biomass burning	Young biomass burning	Haze	0.2	No
Rural background	Rural background	Rural background	0.5	No
Marine with continental influence	Marine with continental influence	Marine with continental influence	0.5	No
<i>Cold cases</i>				
Biomass burning Scenario 1	Young biomass burning	Haze	0.2	Biological $d > 0.4 \mu\text{m}$
Biomass burning Scenario 2	Young biomass burning	Haze	0.2	Mineral
Biomass burning Scenario 3	Young biomass burning	Haze	0.2	Soot $d < 0.2 \mu\text{m}$

Initial aerosol particle (AP) distributions for the air parcel and the environment, soluble fraction  $\varepsilon$  of the aerosol particles, and sort of ice nuclei (IN) are listed.

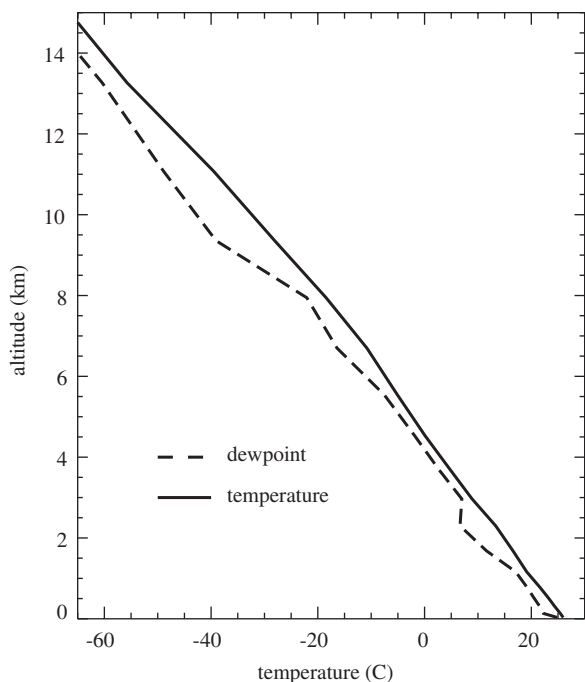


Fig. 1. Vertical profiles of dew point and temperature for a biomass burning situation as used as model input (B. Langmann, personal communication, 2004).

area. They found mainly three components with average fractions of approximately 60% for pyrogenic particles, 15% for soil dust, and 25% for natural biogenic organics. Around half of the pyrogenic fraction consists of carbon (total carbon TC); perhaps the tenth part of TC is black carbon, i.e., soot. Natural biogenic organics come from two main sources: primary biological particles and gas-

to-particle conversion from biogenic volatile organic compounds (VOCs); it can be roughly estimated that less than half of the biogenic compound consists of primary biological particles as pollen, leaf litter, bacteria, lichen, fungi (all estimations based on Guyon et al., 2003). It was taken into account that Guyon et al. (2003) and Artaxo et al. (1998) gave values in mass percent while for the model simulations number percent were needed: black carbon particles are in the fine mode, biological particles in the coarse mode; therefore, the mass percent were doubled in case of black carbon but halved in case of the biological particles. From these estimations the following number fractions were deduced: 10% for soot particles, 5% for biological particles, and 15% for mineral particles. Soot, biological particles, and mineral dust were allowed to act as ice nuclei in immersion and contact modes according to their specific ice nucleating efficiencies as given in Diehl and Wurzel (2004) and Diehl et al. (2006). Pollen and kaolinite, respectively, were selected as representatives for biological and mineral particles. The following constants in Eqs. (1) and (2) were used: for pollen  $B_{h,i} = 1.01 \times 10^{-2} \text{ cm}^{-3}$ ,  $a_{h,c} = 0.0864 \text{ }^\circ\text{C}^{-1}$ ,  $b_{h,c} = 0.5629$ ; for kaolinite  $B_{h,i} = 6.15 \times 10^{-8} \text{ cm}^{-3}$ ,  $a_{h,c} = 0.1007 \text{ }^\circ\text{C}^{-1}$ ,  $b_{h,c} = 0.6935$ ; for soot  $B_{h,i} = 2.91 \times 10^{-9} \text{ cm}^{-3}$  (according to Diehl et al., 2006). For contact freezing of soot particles in the fine mode a new parameterization was used based on the experimental results of Gorbunov et al. (2001); the constant values were  $a_{h,c} = 0.010 \text{ }^\circ\text{C}^{-1}$  and  $b_{h,c} = 0.977$ . Some restrictions were made regarding the particle sizes. According to Guyon et al. (2003)

mineral dust particles were found in the coarse and fine mode while black carbon was found in the fine mode only. Biological particles such as bacteria, spores, pollen and plant fragments generally show sizes larger than  $0.4\ \mu\text{m}$  in diameter (Matthias-Maser, 1998). Therefore, it was assumed that soot ice nuclei had to be smaller than  $0.2\ \mu\text{m}$ , biological ice nuclei larger than  $0.4\ \mu\text{m}$  in diameter while mineral ice nuclei were allowed in the whole size range. The following scenarios were simulated: scenario 1 including 5% biological ice nuclei, scenario 2 including 15% mineral ice nuclei, scenario 3 including 10% soot ice nuclei, and warm cases without drop freezing.

For comparisons model simulations of warm cases were undertaken with two more dry aerosol particle size distributions: a rural background

distribution (Jaenicke, 1988) and a marine distribution with continental influence (Hoppel and Frick, 1990; Hoppel et al., 1990). The parameters of these distributions are given in Table 1. In these two cases the soluble fraction of the aerosol particles was set to a mean value of  $\varepsilon = 0.5$ ; see also Table 2.

## 4. Results and discussion

### 4.1. Liquid drop distributions and effective radii (warm cases)

Fig. 2 shows the evolution of the cloud drop diameter distribution with altitude in 1000, 2000, and 4000 m above ground level (with temperatures still above  $0^\circ\text{C}$ ) for different aerosol particle size distributions. It is obvious that for all cases the

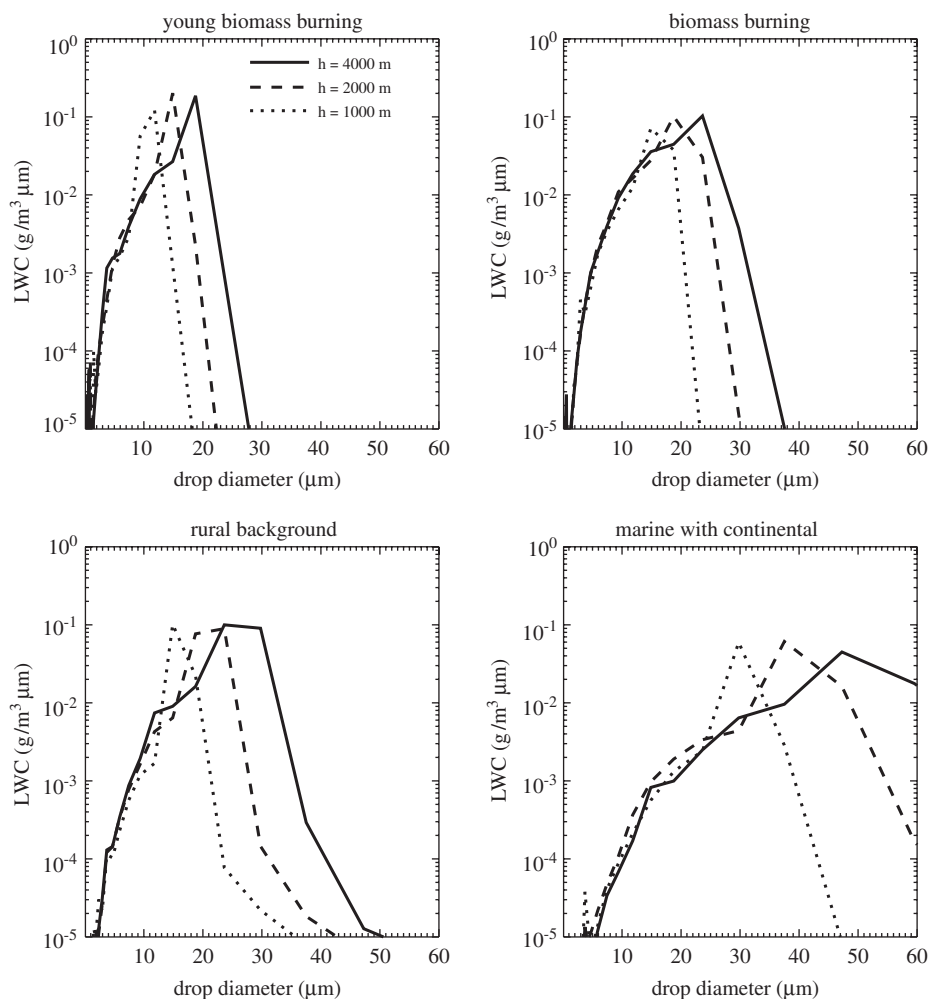


Fig. 2. Liquid water content in  $\text{g}\ \text{m}^{-3}\ \mu\text{m}^{-1}$  as function of drop diameter in  $\mu\text{m}$  for different altitudes and aerosol particle number size distributions.

cloud drop diameter distributions broadened with height, i.e. the drop size increased by condensation and entrained aerosol particles were activated to further drops. However, for the biomass burning cases the cloud drop diameter distributions stayed rather narrow while they developed to wide distributions in case of background conditions and especially in case of marine conditions. Note here that in the nonbiomass burning cases where precipitation-sized drops formed the sizes of these were overestimated. As they cannot fall out from the air parcel the precipitation-sized drops grew further by collision and coalescence. The calculated distributions could be compared with results from Andreae et al. (2004) who made satellite observations over regions with vegetation fires in so-called smoky and pyro clouds, over the “green” and the “blue” ocean. One notices a very good agreement indicating that the present model simulations for young biomass burning conditions could represent a pyro situation, for biomass burning conditions a smoky cloud, for background conditions the green ocean, and for marine conditions the blue ocean rather well. The narrow drop distributions for the biomass burning situations indicate the suppression of warm rain.

The parameter which is mentioned in discussions about suppression of warm rain is the effective radius of the liquid drops. Rosenfeld and Gutman (1994) showed that the formation of rain drops by colliding cloud drops is greatly reduced when the effective drop radius is smaller than a threshold of  $14\ \mu\text{m}$ . According to satellite observations convective clouds forming in regions with vegetation fires show significantly reduced drop sizes as compared to regions without fires. These reductions of cloud drop sizes lead to the suppression of warm precipitation in lower altitudes (Rosenfeld, 1999). The variation of the effective radius with temperature and altitude for the warm case, i.e. without ice formation, is given in Fig. 3 for smoky conditions, i.e. for young biomass burning and biomass burning, and for pure conditions, i.e. background and marine. Very similar as it was observed by Rosenfeld (1999) in the present model simulations the effective radius of the liquid drops stayed below the threshold of  $14\ \mu\text{m}$  for smoky conditions but exceeded the  $14\ \mu\text{m}$  threshold for clean conditions.

#### 4.2. Ice formation

According to Rosenfeld (1999) and Andreae et al. (2004), clouds over regions with vegetation fires

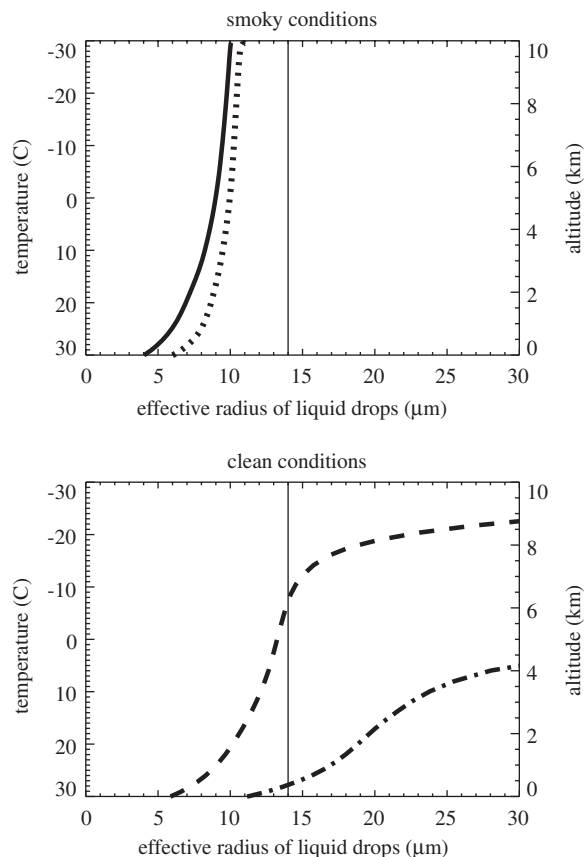


Fig. 3. Variation of the effective radius with temperature and altitude for the warm case with different aerosol particle distributions. Solid line: young biomass burning, dotted line: biomass burning, dashed line: rural background, dashed-dotted line: marine with continental influence. Thin vertical line:  $14\ \mu\text{m}$  threshold.

have to exceed the freezing level to start precipitating, i.e. to increase the effective radius of the cloud particles to more than  $14\ \mu\text{m}$ . However, the onset of freezing will lead again to a reduction of the effective radius of the remaining liquid drops because of the preferential freezing of large drops (Pruppacher and Klett, 1997). It was shown in Diehl et al. (2006) that contact freezing could be very efficient for cases with a high insoluble fraction of the aerosol particles which is the case for a biomass burning situation. Contact freezing starts at rather similar temperatures for all ice nuclei while in the immersion mode the onset of freezing strongly differs in dependence of the ice nuclei type. Lowering the temperature leads to the freezing of more and smaller drops via immersion freezing while in the contact mode the collision efficiency between super-cooled drops and the ice nuclei is the ruling

factor, i.e. lowering the temperature further does not necessarily lead to an increasing number of ice particles but rather to the growth of the ice particles at the expense of liquid drops. With this knowledge the results of the present model simulations are interpreted.

For the three scenarios the vertical profiles of super-saturations respective to liquid water (solid lines) and of super-saturations respective to ice (dashed lines) are given in Fig. 4, left panel; the right panel shows the vertical velocities of the air parcel. These parameters of cloud dynamics and humidity compare to observations in convective clouds (see, e.g., Mason, 1971; Ludlam, 1980; Pruppacher and Klett, 1997). Figs. 5 shows results from the present model simulations including the ice phase compared to the warm case. The total numbers of liquid (solid lines) and frozen drops (dotted lines) for the different scenarios are given in Fig. 5. In the warm case, the air parcel, i.e. the cloud, reached a temperature of  $-30^{\circ}\text{C}$  only. Due to the release of latent heat the lifetime of the cloud could be enhanced by efficient freezing depending on the simulated scenarios. This was not the case for scenario 3, i.e. with soot particles as ice nuclei, where a rather low number of ice particles formed. The profile of the vertical velocity in Fig. 4, right panel, reflects this fact: it shows one maximum only, i.e.  $15\text{ m s}^{-1}$  at 5 km height, which is associated to condensation and droplet formation. Freezing was first induced by contact freezing followed by a small second increase due to immersion freezing when the temperature lowered (see Fig. 5), however, the release of latent heat was too little to affect an enhanced updraft of the cloud (see Fig. 4, right panel).

Freezing via mineral particles as ice nuclei (scenario 2) enhances the number of frozen drops by an order of magnitude. Freezing was first induced by contact freezing followed by a second increase due to immersion freezing when the temperature lowered (see Fig. 5). The amount of ice formed was large enough so that the release of latent heat led to a longer lifetime of the cloud and to an increased vertical updraft of the cloud so that temperatures down to  $-40^{\circ}\text{C}$  were reached. This is indicated also in Fig. 4, right panel: After the first maximum at 5 km height the vertical velocity increased again at 9.5 km height reaching a second small maximum of  $4.5\text{ m s}^{-1}$  at 10.5 km height which is due to enhanced drop freezing via immersion freezing (see also discussion below).

The number of frozen drops was dramatically enhanced during scenario 1 where biological particles acted as ice nuclei leading to an even more increased vertical updraft of the cloud so that temperatures down to  $-55^{\circ}\text{C}$  were reached. Contact freezing was mostly suppressed because of the large particle sizes but immersion freezing affected the significant increase of frozen drops. The profile of the vertical velocity reached a second maximum of  $10\text{ m s}^{-1}$  at 10.5 km height due to efficient immersion freezing of drops. However, in real clouds ice particle numbers of more than  $10\text{ per cm}^3$  are found only under exceptional conditions (e.g., in convective cells of tropical clouds, see Heymsfield et al., 2005). Generally, for convective complexes of clouds ice particle concentrations up to  $10^{-1}\text{ cm}^{-3}$  are found; see Pruppacher and Klett (1997), Figs. 2-42 and 2-43. Thus, the simulation of scenarios 2 and 3 led to more realistic ice particle concentrations than scenario 1.

The liquid drop numbers formed during the ascent of the air parcel reached around  $2000\text{ per cm}^3$  which is in excellent agreement with measurements of Andreae et al. (2004) for smoky conditions. With rising numbers of ice particles the number of liquid drops strongly decreased indicating that the cloud was completely glaciated in scenarios 1 and 2. As shown in Fig. 4, the super-saturation with respect to water dropped below 0 at 8.5 km height (i.e. at  $-23^{\circ}\text{C}$ , see Fig. 1) for scenario 1 and at 10.5 km height (i.e. at  $-35^{\circ}\text{C}$ , see Fig. 1) for scenario 2. As can be seen from Fig. 5, no liquid drops were available in these altitudes. The fact that the ice particle numbers did not reach the liquid drop numbers even for complete glaciation of the cloud indicates that the frozen drops grew by deposition of water vapor at the expense of liquid drops (Bergeron–Findeisen process) or by riming, i.e. the deposition of liquid drops on the ice particles. From Fig. 4, left panel, one notices that the super-saturation respective to ice was significantly higher than the super-saturation respective to liquid water as long as liquid drops were available. This difference is strong evidence that the Bergeron–Findeisen process took place. If frozen drops grow by the deposition of water vapor only the particle mass inside them will stay constant. However, this was not the case in the present simulations: the particle mass inside the frozen drops increased during the whole ascent of the air parcel (results not shown here). Thus, it can be concluded that both growth processes took place

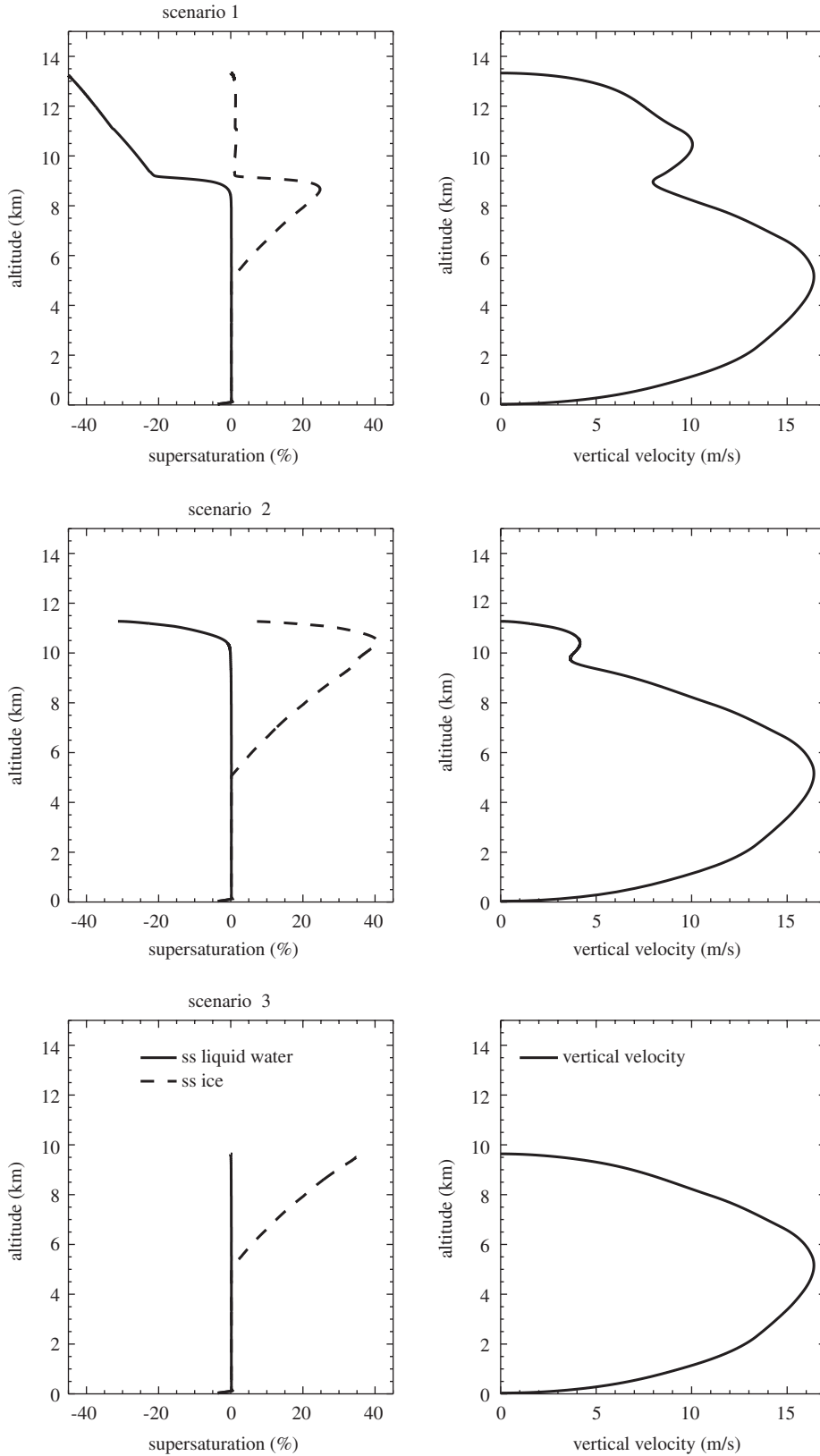


Fig. 4. Left panel: vertical profiles of super-saturations respective to liquid water (solid line) and of super-saturations respective to ice (dashed line); right panel: vertical velocities in  $\text{m s}^{-1}$ ; for three scenarios including the ice phase.

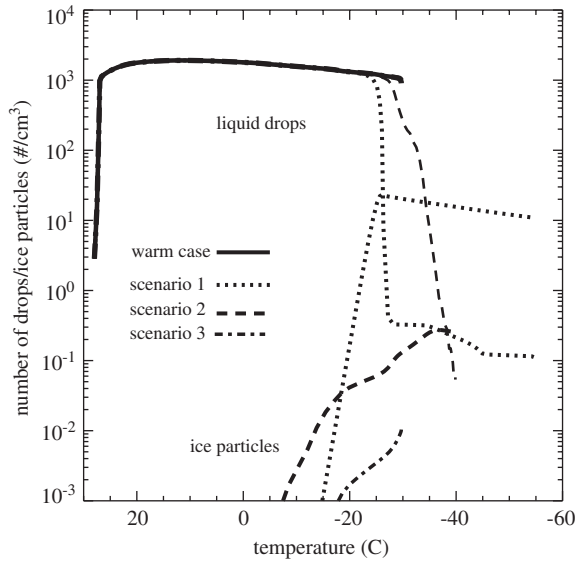


Fig. 5. Total number of liquid drops and ice particles per  $\text{cm}^3$  as function of temperature for the warm case and different scenarios including the ice phase.

simultaneously leading to the complete glaciation of the cloud in scenarios 1 and 2. This is proven in Fig. 6 where the liquid and the ice water content for the same cases as in Fig. 5 are given. For scenarios 1 and 2 the ice water content reaches the liquid water content which in turn decreases indicating that the cloud is completely glaciated. This was not the case for scenario 3. The relatively small decrease of quantities with temperature, i.e. with altitude, in Figs. 5 and 6 resulted from the entrainment where particle numbers did not decrease with height.

For all three scenarios, Fig. 7 shows the change of the effective radius of liquid and frozen drops with temperature and altitude; ice particle size distributions at various temperatures are given in Fig. 8. For scenario 3 where soot particles were allowed as ice nuclei the frozen drop effective radius increased significantly at temperatures below  $-20^\circ\text{C}$  indicating the growth of frozen drops by the deposition of water vapor and by riming. Since the ice particle number was very small these few particles could grow fast almost without competition. However, the liquid drop effective radius was not affected by freezing and reached nearly  $11\ \mu\text{m}$  at  $-30^\circ\text{C}$  and 9.5 km as in the warm case (see Fig. 3). From Fig. 8 one notices that the ice particle size distribution quickly developed from a narrow distribution at  $-15^\circ\text{C}$  to a broad one at  $-25^\circ\text{C}$ .

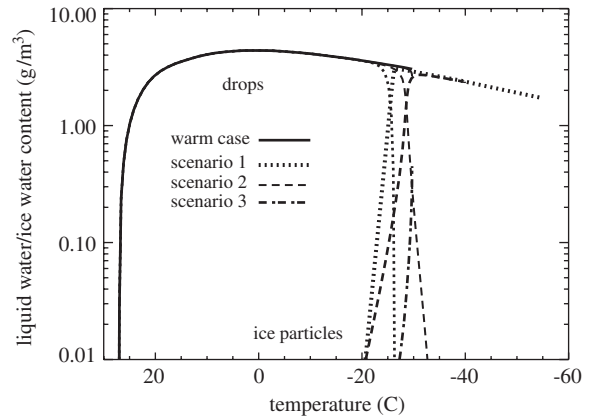


Fig. 6. Liquid and ice water content in  $\text{g m}^{-3}$  as function of temperature for the warm case and different scenarios including the ice phase.

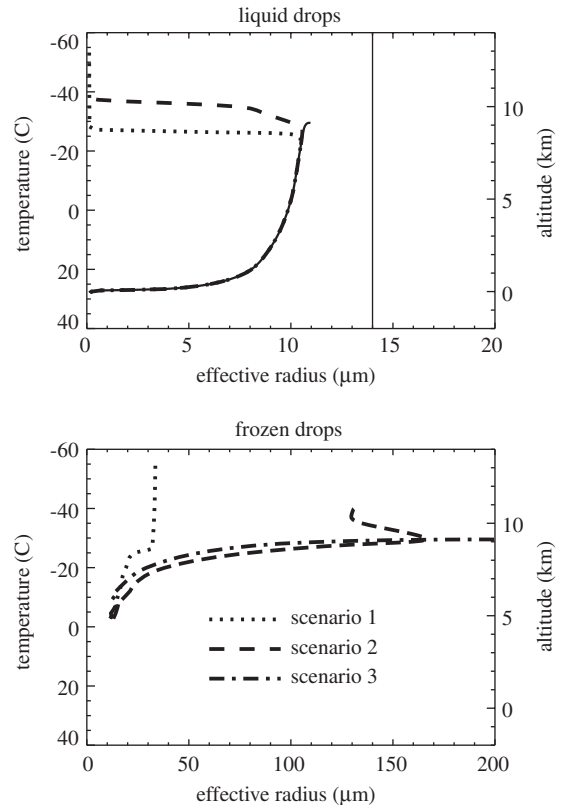


Fig. 7. Variation of the liquid and frozen drop effective radius with temperature and altitude. Upper panel: solid line is for warm case and scenario 3. Thin vertical line:  $14\ \mu\text{m}$  threshold.

For scenario 2 where mineral particles acted as ice nuclei the larger ice amount affected an updraft of the cloud to higher altitudes around 11 km with

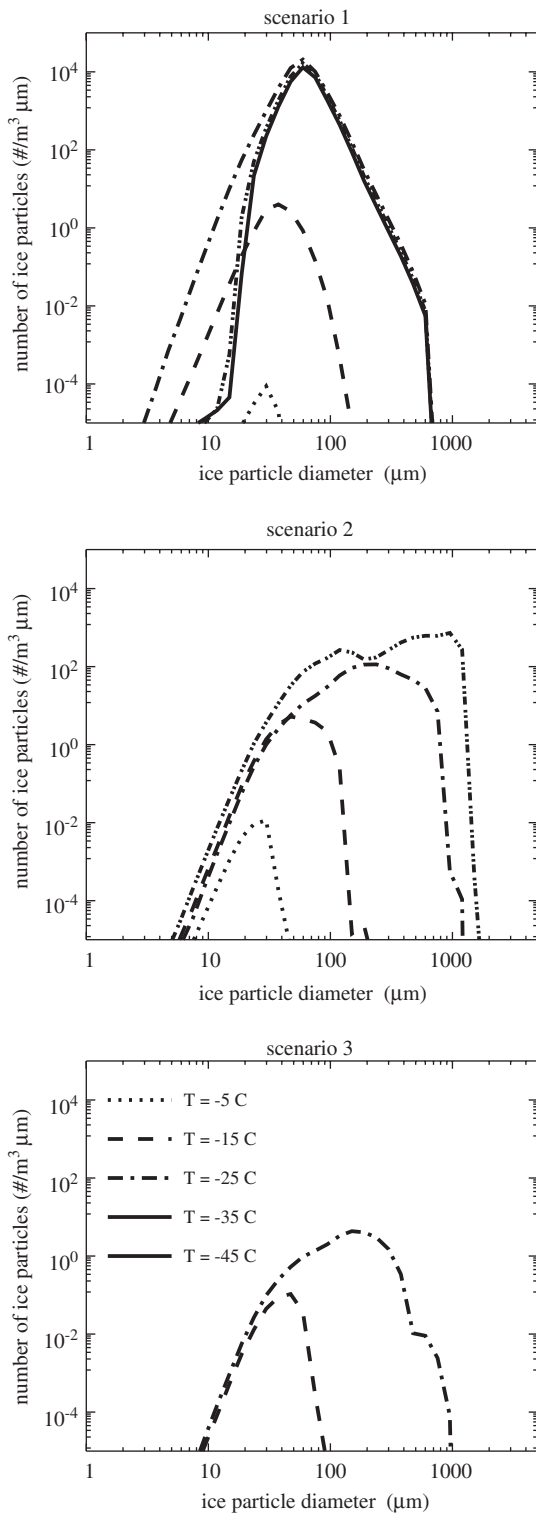


Fig. 8. Number of ice particles per  $\text{m}^3 \mu\text{m}$  as function of drop diameter in  $\mu\text{m}$  for different temperatures and three scenarios.

temperatures down to  $-40^\circ\text{C}$ . At temperatures below around  $-27^\circ\text{C}$  the liquid drop effective radius continuously decreased because of the preferential freezing of large drops, riming (i.e., ice particles collide more efficiently with larger drops than with smaller ones), and the evaporation of liquid drops due to the Bergeron–Findeisen process. The frozen drop effective radius significantly increased at temperatures lower than  $-15^\circ\text{C}$ , reached a maximum at  $-30^\circ\text{C}$  and decreased afterwards. The latter decrease is caused by the onset of immersion freezing at a temperature of approximately  $-27^\circ\text{C}$  (see Fig. 5): the lower the temperature the smaller drops freeze (Diehl and Wurzler, 2004). Looking at the ice particle size distribution in Fig. 8 these conclusions are validated. The narrow ice particle size distribution at  $-5^\circ\text{C}$  slowly developed to a broad one at lower temperatures. There were larger as well as smaller ice particles present than in scenario 3. The larger ice particles formed during the longer updraft of the cloud, the smaller ice particle formed by more efficient immersion freezing. Between  $-25$  and  $-35^\circ\text{C}$  a second maximum at around  $100 \mu\text{m}$  developed by immersion freezing.

For scenario 1 with biological particles as ice nuclei the cloud reached an altitude of approximately  $13 \text{ km}$  with temperatures around  $-55^\circ\text{C}$ . The liquid drop effective radius decreased dramatically at a temperature around  $-25^\circ\text{C}$ . On the other hand, the frozen drop effective radius increased rather slowly with a clear enhancement around  $-25^\circ\text{C}$ ; afterwards, however, it stayed rather small. This is affected by immersion freezing leading to the freezing of more and smaller drops with lower temperatures (Diehl et al., 2006) which is visible in Fig. 8, too. The ice particle size distribution developed towards smaller sizes during the temperature decrease to  $-25^\circ\text{C}$ . At lower temperatures, where no more liquid drops were available (see Figs. 5 and 6) smaller ice particles vanished but larger ones did not form. One can conclude from Fig. 4 that at these lower temperatures small ice particles evaporated because the super-saturation respective to ice decreased. So the ice particle size distribution stayed narrow even for low temperatures with a maximum at definitely smaller sizes as for scenarios 2 and 3. Thus, for scenario 1 larger ice particles which could serve as germs for graupel and hailstone formations were not found which is in contrast to the observations of Andreae et al. (2004) who observed graupel and hailstones in biomass

burning regions. This is due to the overestimation of ice particle number and the so-induced competition effect among the frozen drops which limits the depositional growth. Note here that typically the formation of large hailstones needs several vertical cycles through the cloud; however, this cannot be provided by a parcel model due to dynamic limitations.

## 5. Conclusions

The present model simulations describe well the situation in clouds over a region with biomass burning. In comparison to background or marine conditions the liquid drop effective radius stayed below the critical value of 14  $\mu\text{m}$  for biomass burning cases indicating the suppression of warm rain as observed by Rosenfeld (1999). The simulated development of the cloud size spectrum with altitude behaved similar to that observed by Andreae et al. (2004) for different situations. In spite of the small drop sizes heterogeneous drop freezing via immersion and contact modes is very efficient due to the high insoluble fraction of the biomass burning particles. The results of three scenarios with different active ice nuclei indicated that scenario 1 with biological particles as ice nuclei overestimates the ice particle number concentration. Andreae et al. (2004) observed the formation of graupel and hailstones in biomass burning clouds but in scenario 1 the ice particles did not grow to larger sizes due to the overestimation of their number. Thus, this scenario has to be assumed as unrealistic. It is possible that the biological particles lose their efficient freezing ability by biomass burning. As it has been shown by Hazra et al. (2004) the proteins responsible for efficient ice nucleation of bacteria and leaf litter are destroyed at high temperatures; this might be the case for other biological particles, too. Scenario 3 where soot particles are allowed to act as ice nuclei probably also gives rather unrealistic results as the amount of ice is too low to affect the vertical cloud dynamics. Thus, it cannot be assumed that soot particles are the only active ice nuclei in biomass burning situations but mineral dust particles have to be included, too. This is proven by scenario 2 with mineral particles as active ice nuclei which seems to represent a realistic case: the vertical dynamics of the cloud is significantly affected, and the ice particles grow to larger sizes which may serve as germs for graupel or hailstone formation while the

liquid drop effective radius decreases at higher altitudes because of the preferential freezing of large drops.

## Acknowledgements

These studies were supported by the Ministry of Research and Education of the Federal Republic of Germany under the EFEU project 07ATF46 within the AFO2000 research program and by the Deutsche Forschungsgemeinschaft under SFB 641: The Tropospheric ice phase. The authors thank Bärbel Langmann (MPI Hamburg) for providing the thermodynamical profiles and two anonymous reviewers for their helpful comments and suggestions.

## References

- Andreae, M.O., Rosenfeld, D., Artaxo, P., Costas, A.A., Frank, G.P., Longo, K.M., Silva-Dias, M.A.F., 2004. Smoking rain clouds over the Amazon. *Science* 303, 1337–1342.
- Artaxo, P., Fernandez, E.T., Martins, J.V., Yamasoe, M.A., Hobbs, P.V., Maenhaut, W., Longo, K.M., Castanho, A., 1998. Large scale aerosol source apportionment in Amazonia. *Journal of Geophysical Research* 103, 837–848.
- Diehl, K., Wurzler, S., 2004. Heterogeneous drop freezing in the immersion mode: Model calculations considering soluble and insoluble particles in the drops. *Journal of Atmospheric Science* 61, 2063–2072.
- Diehl, K., Simmel, M., Wurzler, S., 2006. Numerical sensitivity studies on the impact of aerosol properties and drop freezing modes on the glaciation, microphysics, and dynamics of clouds. *Journal of Geophysical Research*. 111, D07202.
- Feingold, G., Remer, A.A., Ramaprasad, J., Kaufman, Y.J., 2001. Analysis of smoke impact on clouds in Brazilian biomass burning regions: an extension of Twomey's approach. *Journal of Geophysical Research*. 106 (D19), 22907–22922.
- Flossmann, A.I., Hall, W.D., Pruppacher, H.R., 1985. A theoretical study of the wet removal of atmospheric pollutants, Part I: the redistribution of aerosol particles captured through nucleation and impaction scavenging through growing cloud drops. *Journal of Atmospheric Science* 42, 583–606.
- Gorunov, B., Baklanov, A., Kakutkina, N., Windsor, H.L., Toumi, R., 2001. Ice nucleation on soot particles. *Journal of Aerosol Science* 32, 199–215.
- Guyon, P., Graham, B., Beck, J., Boucher, O., Gerasopoulos, E., Mayol-Bracero, O.L., Roberts, G.C., Artaxo, P., Andreae, M.O., 2003. Physical properties and concentration of aerosol particles over the Amazon tropical forest during background and biomass burning conditions. *Atmospheric Chemistry and Physics* 3, 1951–1967.
- Hazra, A., Saha, U.K.De., Mukherjee, J., Goswami, K., 2004. Study of ice nucleation characteristics of *Pseudomonas aeruginosa*. *Aerosol Science* 35, 1405–1414.
- Helsper, C., Fissan, H.J., Muggli, J., Scheidweiler, A., 1980. Particle number distribution of aerosols from test fires. *Journal of Atmospheric Science* 11, 439–446.

- Heymsfield, A.J., Miloshevich, L.M., Schmitt, C., Bansemer, A., 2005. Homogeneous ice nucleation in subtropical and tropical convection and its influence on cirrus anvil microphysics. *Journal of the Atmospheric Sciences* 62, 41–64.
- Hoppel, W.A., Frick, G.M., 1990. Submicron aerosol size distributions measured over the tropical and south Pacific. *Atmospheric Environment* 24A, 45–659.
- Hoppel, W.A., Fitzgerald, J.W., Frick, G.M., Larson, R.E., Mack, E.J., 1990. Aerosol size distributions and optical properties found in the marine boundary layer over the Atlantic Ocean. *Journal of Geophysical Research* 95, 3659–3686.
- Jaenicke, R., 1988. Aerosol Physics and Chemistry. In: Landolt-Bernstein, *Zahlenwerte und Funktionen aus Naturwissenschaften und Technik*. V4B, Springer, New York, pp. 391–457.
- Khain, A.P., Ovtchinnikov, M., Pinsky, M., Pokrovsky, A., Krugliak, H., 2000. Notes on the state-of-the-art numerical modelling of cloud microphysics. *Atmospheric Research* 55, 159–224.
- Koop, T., Bertram, A.K., Molina, L.T., Molina, M.J., 1999. Phase transitions in aqueous  $\text{NH}_4\text{HSO}_4$  solutions. *Journal of Physical Chemistry* 103, 9042–9048.
- Langmann, B., 2004. Calculations with REMO. MPI Hamburg, Germany, pers. comm.
- Levine, J.S. (Ed.), 1991. *Global Biomass Burning: Atmospheric, Climatic, and Biospheric Implications*. The MIT Press, Inc.
- Ludlam, F.H., 1980. *Clouds and Storms: The Behaviour and Effect of Water in the Atmosphere*. Pennsylvania State University Press.
- Mason, B.J., 1971. *The Physics of Clouds*. Clarendon Press, Oxford.
- Matthias-Maser, S., 1998. Primary biological aerosol particles: their significance, sources, sampling methods and size distribution in the atmosphere. In: Harrison, R.M., van Grieken, R.E. (Eds.), *Atmospheric Particles*. Wiley, New York, pp. 349–369.
- Pruppacher, H.R., Klett, J.D., 1997. *Microphysics of Clouds and Precipitation*, 2nd ed. Kluwer, Dordrecht.
- Reid, J.S., Hobbs, P.V., Ferek, R.J., Blake, D.R., Martins, J.V., Dunlap, M.R., Liousse, C., 1998. Physical, chemical, and optical properties of regional hazes dominated by smoke in Brazil. *Journal of Geophysical Research* 103, 32059–32080.
- Rosenfeld, D., 1999. TRMM observed first direct evidence of smoke from forest fires inhibiting rainfall. *Geophysical Research Letters* 26, 3105–3108.
- Rosenfeld, D., Gutman, G., 1994. Retrieving microphysical properties near the tops of potential rain clouds by multi-spectral analysis of AVHRR data. *Atmospheric Research* 34, 259–283.
- Schaller, R.C., Fukuta, N., 1979. Ice nucleation by aerosol particles: experimental studies using a wedge-shaped ice thermal diffusion chamber. *Journal of Atmospheric Science* 6, 1788–1802.
- Simmel, M., Wurzler, S., 2006. Condensation and nucleation in sectional cloud microphysical models. *Atmospheric Research* 80, 218–236.
- Simmel, M., Diehl, K., Wurzler, S., 2005. Numerical simulation of the microphysics of an orographic cloud: comparison with measurements and sensitivity studies. *Atmospheric Environment* 39, 4365–4373.